Eur. Phys. J. B **34**, 231–235 (2003)
DOI: 10.1140/epjb/e2003-00216-2

THE EUROPEAN PHYSICAL JOURNAL B

Nucleation of superconductivity in mesoscopic star-shaped superconductors

D.A. Dikin[1,a], V. Chandrasekhar[1], V.R. Misko[2,b], V.M. Fomin[2,c], and J.T. Devreese[2,d]

[1] Department of Physics and Astronomy, Northwestern University, Evanston, IL 60208, USA
[2] Theoretische Fysica van de Vaste Stoffen, Universiteit Antwerpen (UIA), 2610 Antwerpen, Belgium

Received 26 February 2003
Published online 4 August 2003 – © EDP Sciences, Società Italiana di Fisica, Springer-Verlag 2003

Abstract. We study the phase transition of a star-shaped superconductor, which covers smoothly the range from zero to two dimensions with respect to the superconducting coherence length $\xi(T)$. Detailed measurements and numerical calculations show that the nucleation of superconductivity in this device is very inhomogeneous: the superconducting order parameter is strongly enhanced and mostly robust in regions close to multiple boundaries. The strong inhomogeneity of the order parameter results in a rich structure of the superconducting transition as a function of temperature and magnetic field.

PACS. 74.78.-w Superconducting films and low-dimensional structures – 74.78.Na Mesoscopic and nanoscale systems – 74.20.De Phenomenological theories

Many characteristics of a superconducting sample are strongly influenced by its size with respect to fundamental superconducting length scales. Experimental and theoretical investigations over the past few decades have clearly delineated the differences in behavior between one-dimensional, two-dimensional and "bulk" (three-dimensional) samples as concerns such properties as the critical field, critical temperature and critical current. Recently [1], there has been renewed interest in the effect of sample dimension on the properties of superconductors, fueled in part by their potential use in future nanometer scale devices. The complex geometry of such devices implies that one needs to consider the nucleation of superconductivity over a range of length scales in a single device.

The nucleation of superconductivity in the presence of a magnetic field can be investigated by solving the Ginzburg-Landau(GL) equations for the superconducting order parameter ψ and the vector potential $\mathbf{A}$ of the magnetic field $\mathbf{B} = \nabla \times \mathbf{A}$ [2–4]:

$$\frac{1}{2m}\left(-i\hbar\nabla - \frac{2e}{c}\mathbf{A}\right)^2 \psi + \alpha\psi + \beta\left|\psi\right|^2\psi = 0, \quad (1)$$

$$\nabla^2\mathbf{A} = \frac{4\pi ie\hbar}{mc}\left(\psi^*\nabla\psi - \psi\nabla\psi^*\right) + \frac{16\pi e^2}{mc^2}\mathbf{A}\left|\psi\right|^2 \quad (2)$$

subject to the boundary condition

$$\mathbf{n}\cdot\left(-i\hbar\nabla - \frac{2e}{c}\mathbf{A}\right)\psi = 0. \quad (3)$$

Here α and β is the GL parameters, and $\mathbf{n}$ is the unit vector normal to the surface.

Close to the critical temperature T_c, $|\psi|^2$ is negligible, and one can analytically solve the linearized GL equation (1) for some simple geometries. Saint-James and de Gennes [5] solved this linear equation for the case of a magnetic field parallel to the surface of a superconductor. They found that superconductivity could exist at a field H_{c3} (the so-called surface critical field) larger than the upper critical field H_{c2} in the bulk superconductor, $H_{c3} = 1.69H_{c2}$. More recently [6], attention has focused on superconducting wedges subtending an angle γ, with the magnetic field applied parallel to the wedge's edge. In the limit of small γ, it has been predicted [7,8] that the surface critical field can be greatly enhanced, $H_{c3} = (1.73/\gamma)H_{c2}$, although this has never been demonstrated experimentally. This large enhancement of H_{c3} can be ultimately

[a] *On leave from:* Institute for Low Temperature Physics and Engineering, 61164 Kharkov, Ukraine
[b] *On leave from:* Institute of Applied Physics, 2028 Kishinev, Republic of Moldova
[c] *On leave from:* State University of Moldova, 2009 Kishinev, Republic of Moldova; *Also at:* Technische Universiteit Eindhoven, 5600 MB Eindhoven, The Netherlands
[d] *Also at:* Universiteit Antwerpen (RUCA), B-2020 Antwerpen, Belgium and Technische Universiteit Eindhoven, 5600 MB Eindhoven, The Netherlands
e-mail: devreese@uia.ua.ac.be

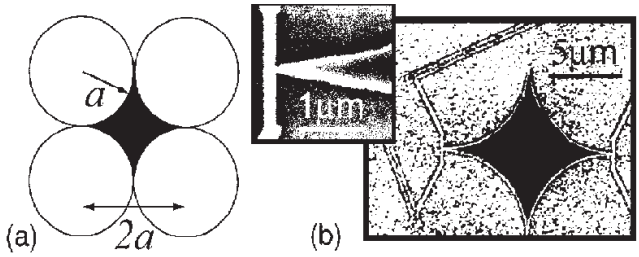

Fig. 1. (a) Schematic representation of the method that was used to design samples. (b) Scanning electron micrograph of one of the samples. The inset shows magnified area of the apex.

traced to the increase in the "energy" $(-\alpha)$ in the GL equation (1) associated with the confinement of the order parameter.

For more complicated geometries, and for regimes further away from the superconducting transition, it is necessary to solve the full GL equations numerically. This has been done for many different geometries, including rings [9,10], square loops [11,12] bridges [13] and triangles [14]. Here we are interested in a four-pointed "star" geometry, shown schematically in Figure 1. The remarkable feature of this geometry is that it encompasses a wide range of length scales. As we shall see, this results in appearance of regions of the sample with characteristically different behavior in the superconducting regime.

The experimental sample is prepared by removing portions of a circle of radius a from the corners of a square of side $2a$, as shown in Figure 1a. The experimental realization of this geometry is shown in Figure 1b. The sample is fabricated by conventional electron beam lithography with a 60 nm thick Al film. The apex-to-apex distance is 12 μm, the minimum dimension at each apex is less than 100 nm. These dimensions are also used in all numerical calculations. In order to enable four-terminal electrical measurements on the device, narrow electrical contacts of the same material are attached to opposite apices.

To obtain the solutions of the GL equations (1), (2) with the boundary conditions (3), we use the finite-difference method applied earlier for the description of superconductivity in a mesoscopic square loop [11,12], using the dimensions and parameters of the experimental sample of Figure 1. One additional complication of this geometry for the finite-difference method is the infinite sharpness of the apices of the "star", which makes the generation of a mesh for the problem difficult. Fortunately, the vertices of the experimental sample have finite curvature, which results in a definite cut-off length of around 100 nm for the tip of each apex, as shown in the inset to Figure 1. In our calculations of the order parameter and magnetic field distributions, a square mesh has been used with the density of 800 nodes per side of the sample. At such a high density of nodes, the results of calculations are independent of the mesh.

The solutions of the GL equations with appropriate boundary conditions permit us to obtain the spatial distribution of the order parameter and the magnetic field

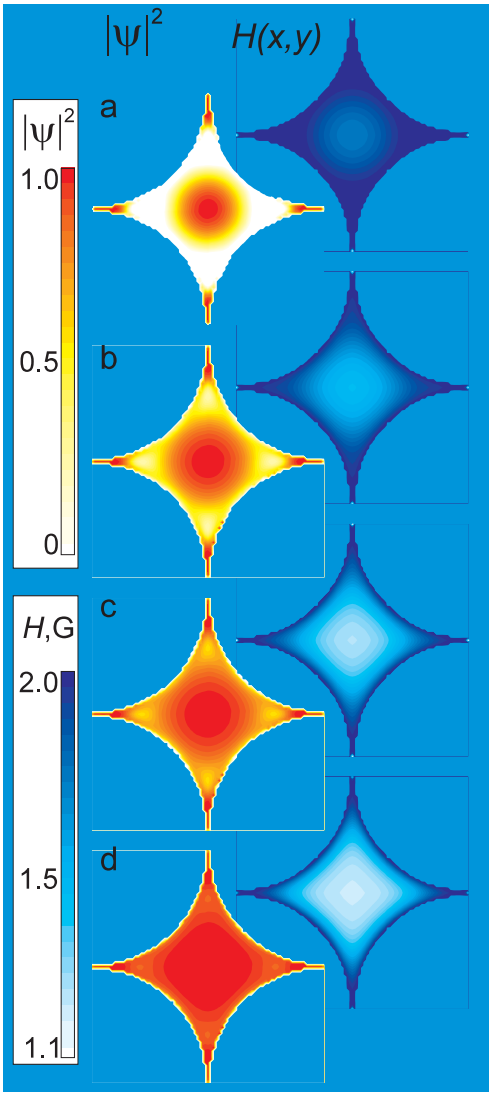

Fig. 2. Evolution of $|\psi(x,y)|^2$ and magnetic field distribution in the "star" with temperature for an applied external field of $H_0 = 0.02H_c(0) = 2$ G, where $H_c(0) = 100$ G is the bulk critical field at zero temperature, at different temperatures: a - $T/T_c = 0.99$, b - 0.98, c - 0.97, d - 0.94. $|\psi(x,y)|^2$ is normalized to its maximum value at these temperatures.

as a function of temperature T, as shown in Figure 2. As temperature is decreased slightly from T_c $(T/T_c = 0.99)$, one observes nucleation of superconductivity as evidenced by a non-zero $|\psi(x,y)|^2$ in two distinct regions of the sample. The first region is a large area in the center, where one might intuitively expect superconductivity to nucleate. The second region is at the apices of the "star", where superconductivity is enhanced by the close proximity of two boundaries, and resembles the situation that occurs in a superconducting "wedge." In between these two regions, $|\psi|^2$ is essentially 0, so that the superconducting phases of the sample are separated by regions of normal phase. The plot of the field distribution shows that the two

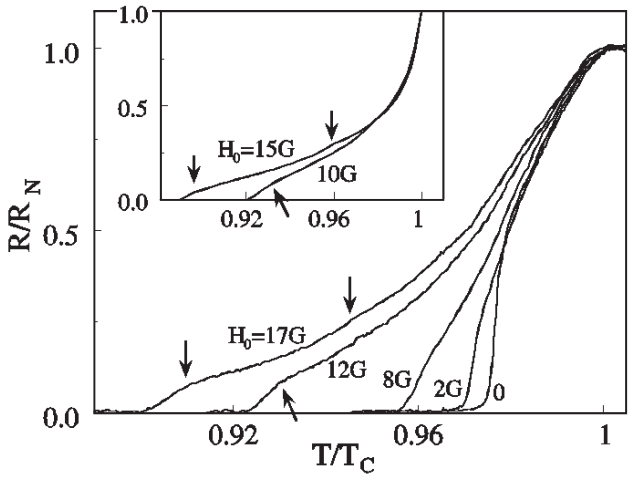

Fig. 3. Experimentally measured resistive transition, taken at different magnetic fields. The inset shows the numerically calculated $R(T)$. $T_c = 1.32$ K, and $R_N = 12\ \Omega$. The "kinks" (denoted by the arrows) define a crossover between different types of the $|\psi(x,y)|^2$-distributions. At low resistances close to $R = 0$, this is the transition from the $|\psi(x,y)|^2$-pattern of the type represented in Figure 2d to that one displayed in Figure 2c. The second "kink", observed at higher resistances, is related to the transition between the $|\psi(x,y)|^2$-patterns of the types plotted in Figures 2b and 2a.

superconducting regions are characterized by different behavior in a magnetic field: the central region shows the beginning of Meissner expulsion of the external field, while the magnetic field near the boundaries is very close to the external field value. As the temperature is lowered further, the superconducting areas in the two regions grow as expected to cover almost the entire sample, and the normal regions between the apices and the center disappear. At the lowest temperature shown, the value of $|\psi|^2$ at the apices and in the central region achieves its maximum corresponding to this temperature, $|\psi(x,y)|^2_{max} \sim (1 - T/T_c) = 0.06$. The magnetic field at the center is greatly reduced, showing the presence of a strong Meissner effect, but the magnetic field in a narrow region at the boundaries of the sample is still very close to the external field value. It should be noted that the value of $|\psi|^2$ at the apices is a maximum, even though the magnetic field is also a maximum. In fact, the value of $|\psi|^2$ at the apices does not change appreciably over the temperature range shown in Figure 2, demonstrating vividly the fact that superconductivity is the most robust in regions close to multiple boundaries.

The electrical contacts in the sample are placed at opposite apices, so that the electrical current must traverse these apices, the central region, as well as any normal regions in between. Consequently, the inhomogeneous nature of superconductivity nucleation as the sample is cooled through its transition imparts a distinctive shape to $R(T)$, as shown in Figure 3. The normal-to-superconducting transition starts with a decrease in resistance over a relatively broad range in temperature even at $H_0 = 0$. In this temperature range, superconductivity begins to nucleate at the apices and at the central part, as was shown in Figure 2, but the regions near the apices, being narrower, contribute a large fraction to the resistance change. As the temperature is reduced further, there is a much sharper drop in the resistance when R is a little less than half the normal state resistance R_N (at $H_0 = 0$). Since the central region and the apices are already superconducting, this rapid change corresponds to the normal-to-superconducting transition of the "necks" between the apices and the central region. Calculations of the superconducting transition confirm this picture.

Numerically, we calculate the resistance of the sample using the order parameter distribution. As the order parameter and magnetic field distributions, the resistance of the sample is calculated on a rectangular mesh. The resistance of a mesh cell in the sample is determined by the value of $|\psi(x,y)|^2$ in the cell, being zero if $|\psi(x,y)|^2 > 0$, and equal to the normal state resistance if $|\psi(x,y)|^2 = 0$. One must also take into account the Josephson coupling between the superconducting regions, which reduces the resistance of the "necks". We suppose that a region of the normal metal of length $\leq p\xi$ (where $p \approx 2$ is an adjustable parameter) between superconducting "islands" does not contribute to the resistance in the circuit. The inset of Figure 3 shows the results of this calculation for two different field values. The theoretical curves reproduce the main qualitative features of the experimental curves, including the "kinks" at low resistances, and are in reasonably good quantitative agreement as well. The appearance of "kinks" in the resistive transition can be interpreted in terms of the inhomogeneous depression of the order parameter in the "star" with rising temperature. The "kinks" at low resistances, which correspond to a crossover from the $|\psi(x,y)|^2$-pattern of the type represented in Figure 2d to that one shown in Figure 2c, can be attributed to the occurrence of areas with strongly depressed order parameter between the central region and the apices. The second (less pronounced) "kink" at a higher resistance, which corresponds to a transition between the $|\psi(x,y)|^2$-patterns of the types plotted in Figsures 2b and 2a, can be related to the ultimate separation of the central superconducting region from the surface superconducting sheath connected to the superconducting regions near the apices. The calculated position of the beginning of the resistive transition compares rather well with the experimental curves when the tunneling of the superconducting electrons through the normal metal is taken into consideration.

The behavior of the sample in a magnetic field (Fig. 4) exhibits even more distinctly the difference between the nature of the superconductivity in the center and in the apices. While $|\psi(x,y)|^2$ in the central region is rapidly attenuated with increasing magnetic field, its value in the apices does not show a large change. At large magnetic fields, only the apices are superconducting. This would imply that the contribution to the resistance of the sample from the apices is not strongly affected by magnetic field.

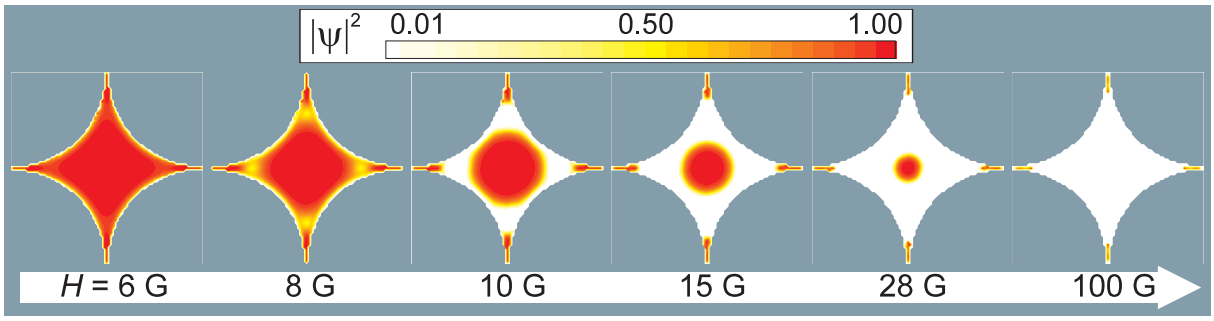

Fig. 4. Evolution of $|\psi(x,y)|^2$ with magnetic field at $T/T_c = 0.96$; $|\psi(x,y)|^2$ is normalized to its maximum value at this temperature.

Evidence for this can be seen directly in the experimental transition curves. The resistance of the sample at the top of the transition, where the decrease in resistance is primarily due to the nucleation of superconductivity in the apices, shows only a weak dependence on magnetic field. At lower values of resistance, where one has contributions from the central region as well as the "necks", the field dependence is much stronger, reflecting the two-dimensional nature of the superconductivity in these regions.

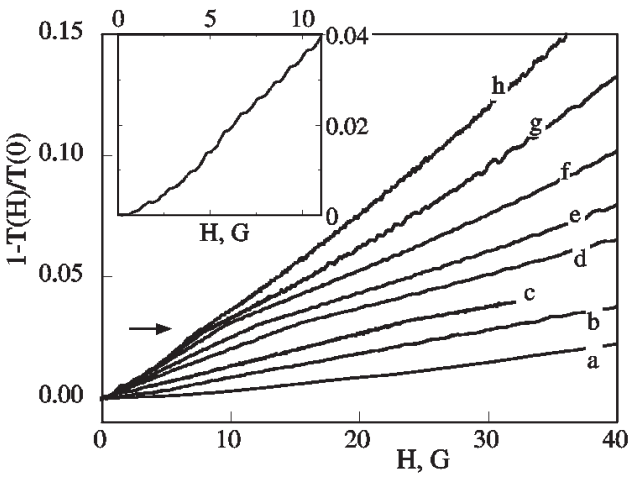

Fig. 5. $T-H$ phase diagrams measured at $R/R_N = 0.58$ (a), 0.42 (b), 0.33 (c), 0.25 (d), 0.21 (e), 0.17 (f), 0.125 (g), 0.08 (h). Inset shows the Little-Parks [15] oscillations at smaller field for $R/R_N = 0.04$.

Even more striking is the magnetic phase diagram (T_c *vs.* H) of the sample. Typically, this is obtained by varying the temperature to maintain the resistance of the sample at the midpoint of the transition ($R/R_N = 0.5$) while changing the magnetic field. Since our sample is inhomogeneous, and it is not clear how one would define the unique T_c, we have measured the phase diagram with the sample biased at various points R/R_N of the superconducting transition. Figure 5 shows the result of these measurements. Although the curves are different, each one shows two distinct regions, separated by a well-defined "kink" denoted by the arrow. At low fields, the curves show a quasi-linear dependence on H_0, which turns into a quadratic dependence at higher magnetic fields. It is well known that the critical temperature of a superconductor varies linearly with the magnetic field in two dimensions, and quadratically in one dimension [4]. The "kink" in each curve defines the crossover from two-dimensional behavior at low fields to one-dimensional behavior at higher fields. This behavior is in agreement with the evolution of the superconducting regions of the sample shown in the numerical simulations of Figure 2. At low fields, the central region and the "necks" of the sample are superconducting, giving a two-dimensional characteristic to the phase diagram. At higher fields, superconductivity in these regions is attenuated, leaving a finite order parameter only in the apices, which gives rise to a quadratic dependence on the magnetic field. It is interesting to note that the low-field linear behavior of all the curves extrapolates to a single temperature at $H_0 = 0$, while the high-field quadratic behavior of all the curves also extrapolates to a single (but different) temperature. The different temperatures clearly point out the inhomogeneous nature of the superconducting transition in this device. Well pronounced T_c oscillations on the magnetic phase diagram, which have been measured at the lowest resistance set point, shown in the inset to Figure 5, imply the presence of the magnetic vortices in our sample. This fact may determine the low temperature resistive "kink", indicated in Figure 3. However, the formation and dynamics of vortices require a separate detailed study, which was beyond the goals of the present paper.

In conclusion, we have analyzed the resistive transition in a star-shaped sample, which combines properties of two-dimensional and zero-dimensional superconductors in a unique manner. Occurrence of qualitatively different regions in the resistive transition reflects a smooth change from 2D to 0D superconducting regime when increasing applied magnetic field or temperature.

We thank V.V. Moshchalkov for valuable discussions. This work was supported at Northwestern University by the National Science Foundation through grant DMR-0201530 and by

the David and Lucile Packard Foundation, and at Universiteit Antwerpen by the IUAP, the GOA BOF UA, the FWO-V, WOG (Belgium) and the ESF Programme VORTEX.

References

1. V.V. Moshchalkov, L. Gielen, C. Strunk, R. Jonckheere, X. Qiu, C. Van Haesendonck, Y. Bruynseraede, Nature **373**, 319 (1995)
2. V.L. Ginzburg, L.D. Landau, Zh. Eksp. Teor. Fiz. **20**, 1064 (1950)
3. P.G. de Gennes, *Superconductivity of Metals and Alloys* (Addison-Wesley, Massachusetts, 1989)
4. M. Tinkham, *Introduction to Superconductivity*, 2nd edn. (McGraw Hill, New York, 1996)
5. D. Saint-James, P.G. de Gennes, Phys. Lett. **7**, 306 (1963)
6. V.M. Fomin, J.T. Devreese, V.V. Moshchalkov, Europhys. Lett. **42**, 553 (1998); **46**, 118 (1999)
7. A. Houghton, F.B. McLean, Phys. Lett. **19**, 172 (1965)
8. A.P. Van Gelder, Phys. Rev. Lett. **20**, 1435 (1968)
9. V.A. Schweigert, F.M. Peeters, P.S. Deo, Phys. Rev. Lett. **81**, 2783 (1998)
10. V.A. Schweigert, F.M. Peeters, Phys. Rev. B **60**, 3084 (1999)
11. V.M. Fomin, V.R. Misko, J.T. Devreese, V.V. Moshchalkov, Solid State Comm. **101**, 303 (1997)
12. V.M. Fomin, V.R. Misko, J.T. Devreese, V.V. Moshchalkov, Phys. Rev. B **58**, 11703 (1998)
13. V.R. Misko, V.M. Fomin, J.T. Devreese, Phys. Rev. B **64**, 014517 (2001)
14. V.R. Misko, V.M. Fomin, J.T. Devreese, V.V. Moshchalkov, Phys. Rev. Lett. **90**, 147003 (2003)
15. W.A. Little, R.D. Parks, Phys. Rev. Lett. **9**, 9 (1962)